A survey of solar wind conditions at 5 AU: a tool for interpreting solar wind-magnetosphere interactions at Jupiter

Robert W. Ebert[1]*, Fran Bagenal[2], David J. McComas[1,3] and Christopher M. Fowler[2]

[1] Space Science and Engineering Division, Southwest Research Institute, San Antonio, TX, USA
[2] Laboratory for Atmospheric and Space Physics, University of Colorado, Boulder, CO, USA
[3] Department of Physics and Astronomy, University of Texas at San Antonio, San Antonio, TX, USA

We examine Ulysses solar wind and interplanetary magnetic field (IMF) observations at 5 AU for two ∼13 month intervals during the rising and declining phases of solar cycle 23 and the predicted response of the Jovian magnetosphere during these times. The declining phase solar wind, composed primarily of corotating interaction regions and high-speed streams, was, on average, faster, hotter, less dense, and more Alfvénic relative to the rising phase solar wind, composed mainly of slow wind and interplanetary coronal mass ejections. Interestingly, none of solar wind and IMF distributions reported here were bimodal, a feature used to explain the bimodal distribution of bow shock and magnetopause standoff distances observed at Jupiter. Instead, many of these distributions had extended, non-Gaussian tails that resulted in large standard deviations and much larger mean over median values. The distribution of predicted Jupiter bow shock and magnetopause standoff distances during these intervals were also not bimodal, the mean/median values being larger during the declining phase by ∼1–4%. These results provide data-derived solar wind and IMF boundary conditions at 5 AU for models aimed at studying solar wind-magnetosphere interactions at Jupiter and can support the science investigations of upcoming Jupiter system missions. Here, we provide expectations for Juno, which is scheduled to arrive at Jupiter in July 2016. Accounting for the long-term decline in solar wind dynamic pressure reported by McComas et al. (2013a), Jupiter's bow shock and magnetopause is expected to be at least 8–12% further from Jupiter, if these trends continue.

Keywords: solar wind, interplanetary magnetic field, Jupiter's magnetosphere, solar wind-magnetosphere interactions, magnetopause, bow shock, Juno

INTRODUCTION

Jupiter's magnetosphere has been explored by several spacecraft, including seven flyby missions (Pioneer 10 and 11, Voyager 1 and 2, Ulysses, Cassini, and New Horizons) and one orbiter (Galileo), as reviewed in Bagenal et al. (2004). Observations from these spacecraft have uncovered the general morphology of the magnetosphere, whose primary feature is the oxygen and sulfur-rich Io torus that peaks in density at ∼6 jovian radii (1 R_J ∼71492 km), and revealed a host of dynamical processes that occur on timescales of minutes—such as plasma interchange near the Io torus (Kivelson et al., 1997), reconnection driven auroral emissions (Grodent et al., 2003), hours—such as spin period modulated radio emissions (Zarka, 2004), energetic electron injections (Mauk et al., 1998), ultraviolet (UV) auroral brightenings (Clarke et al., 2009) and days—such as reconnection driven particle bursts (Woch et al., 1998), plasmoid ejection (Kronberg et al., 2005), large scale outer boundary motion (McComas et al., 2014). There is strong evidence that a number of these processes are powered by the coupling of magnetospheric plasma and energetic particles, primarily from Io, to the planet's 10 h spin period through Jupiter's magnetic field (see reviews by Khurana et al., 2004; Krupp et al., 2004). Another important, though poorly understood driver is the solar wind. This lack of understanding is primarily due to the absence of a solar wind monitor upstream of the planet at the time of these observations.

To date, the best opportunities to study solar wind interactions at Jupiter stem from *in situ* observations as the above listed spacecraft explored the outer boundaries of the jovian magnetosphere. The Pioneer, Voyager, and Ulysses spacecraft all made several crossings of Jupiter's dayside bow shock and/or magnetopause that showed the location of these boundaries responding strongly to changes in the solar wind dynamic pressure (e.g., Smith et al., 1978; Bridge et al., 1979a,b; Bame et al., 1992a). Near simultaneous two-point measurements by Cassini and Galileo showed the magnetosphere transitioning from an expanded to a compressed state in response an increase in solar wind dynamic pressure and associated interplanetary shock (Kurth et al., 2002);

enhanced radio emissions within the magnetosphere and UV aurora emissions were also observed at the same time (Gurnett et al., 2002). Clarke et al. (2009) reported on aurora observations from the Hubble Telescope in coordination with the New Horizons flyby in 2007 and found evidence of solar wind influence on auroral processes at Jupiter but no definitive correlations. A number of studies have used statistical descriptions of the solar wind at 5 AU and/or modeling to study this interaction (Slavin et al., 1985; Stahara et al., 1989; Walker et al., 2001; Joy et al., 2002; Delamere and Bagenal, 2010; Jackman and Arridge, 2011). More recent discussions have focused on mechanisms controlling the dynamics in the outer magnetosphere. Two competing theories are (i) Dungey cycle type convection where magnetic flux is opened on the dayside and closed in the tail through reconnection, followed by a return flow along the dawn side (e.g., Cowley et al., 2003) and (ii) interactions at the magnetospheric boundary, either by the opening and reclosing of the interplanetary and jovian magnetic fields along the magnetopause (McComas and Bagenal, 2007) or stresses imposed by viscous, Kelvin-Helmholtz type interactions between magnetospheric and solar wind plasma along the magnetopause boundary (e.g., Delamere and Bagenal, 2010). This topic is still under debate (McComas and Bagenal, 2007, 2008; Cowley et al., 2008) and our understanding of how the solar wind influences the dynamics of Jupiter's magnetosphere is far from complete.

In this paper, we examine the solar wind plasma and interplanetary magnetic field (IMF) at ~5 AU, and the predicted response of the Jovian magnetosphere to these external drivers, to deliver a tool for investigating solar wind-magnetosphere interactions at Jupiter. We focus on two ~13-month intervals when the Ulysses spacecraft was near 5 AU and within ±10° of the ecliptic plane, comparing the solar wind and IMF conditions during the rising and declining phases of solar cycle 23. We statistically describe several key solar wind and IMF properties that are expected to contribute to solar wind interactions at Jupiter. We use the model of Joy et al. (2002) and the solar wind dynamic pressures during these intervals to predict the bow shock and magnetopause standoff distances, comparing their distributions for different periods in the solar cycle. These results will provide data-derived solar wind and IMF boundary conditions at 5 AU for models aimed at studying solar wind-magnetosphere interactions at Jupiter and can be used to support the science investigations of upcoming Jupiter system missions such as Juno (Bolton and the Juno Science Team, 2010), JUICE (Dougherty, 2013) and Europa Clipper (Pappalardo et al., 2013). Here, we provide expectations for the solar wind conditions and the state of Jupiter's

magnetosphere during the Juno mission, which is schedule to arrive at Jupiter in July 2016.

OBSERVATIONS

We examine 1-h averaged observations from the Solar Wind Observations Over the Poles of the Sun (SWOOPS; Bame et al., 1992b) plasma instrument and the Vector Helium and Flux Gate magnetometer (MAG; Balogh et al., 1992) experiment onboard the Ulysses spacecraft, focusing on two periods when Ulysses was at ~5 AU and covering a −10° to 10° range in heliolatitudes. The details of these intervals are described in **Table 1**. Both intervals span roughly 13-month timeframes at different periods in the solar cycle and contain >9000 separate 1-h averaged measurements, providing a large sample size to investigate the solar wind properties at ~5 AU.

Figure 1 is a plot of the sunspot number vs. year from 1992 to 2020 and the predicted sunspot number from NASA's Marshall Space Science Center Solar Physics Group, derived using methods described in Hathaway et al. (1994). The sunspot number prediction is updated on a monthly basis and starts to become reliable in a given solar cycle ~3 years after the sunspot minimum of the previous cycle has occurred. Superimposed on the
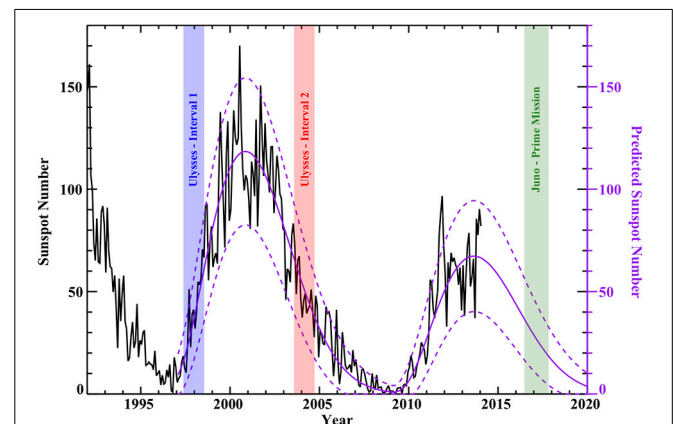

FIGURE 1 | Sunspot number vs. year for the period covering the declining phase of solar cycle 22 through the expected minimum of solar cycle 24. Solid purple line denotes the predicted sunspot number derived using the methods described in Hathaway et al. (1994), the upper and lower dashed purple lines denoting the 95th and 5th percentiles of the prediction, respectively. Blue and red shaded regions identify two timeframes when Ulysses was at ~5 AU and within ±10° of the ecliptic plane. Green shaded region identifies the timeframe of the Juno mission at Jupiter.

Table 1 | Summary of Ulysses observation times used in this study.

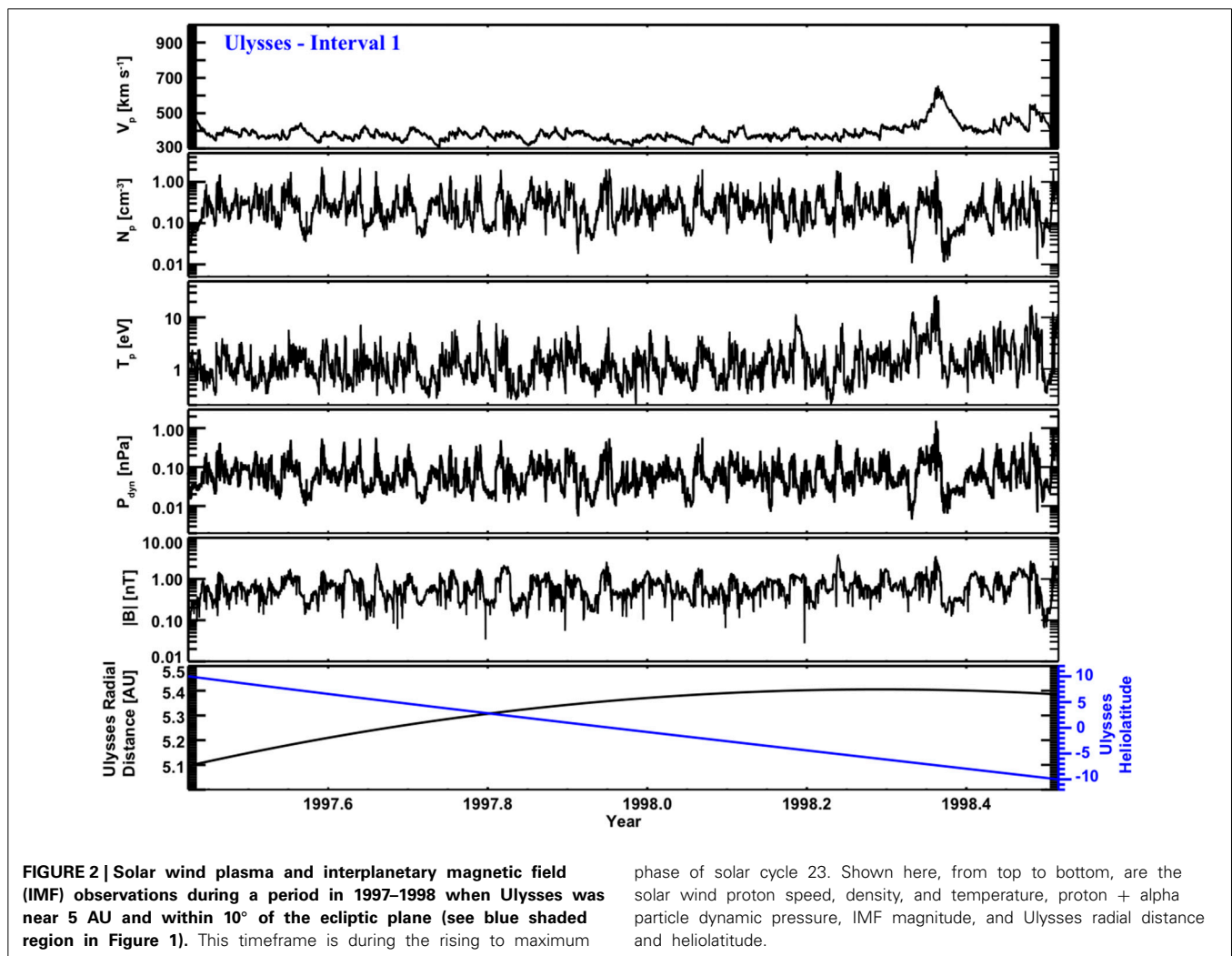| Interval	Period	Radial distance (AU)	Heliolatitude (deg.)	Number of 1-h observations	Solar cycle epoch	Ulysses orbit description
1	06/04/1997 22:30–07/08/1998 03:30	5.10–5.41	±10	9398	Rising to maximum phase of solar cycle 23	End of orbit 1 and start of orbit 2
2	08/14/2003 21:30–09/11/2004 05:30	5.09–5.40	±10	9311	Declining to minimum phase of solar cycle 23	End of orbit 2 and start of orbit 3

plot are the periods covering the two Ulysses intervals described in **Table 1** and the prime phase of the Juno mission. Ulysses interval 1 (blue shaded region) occurred during the rising phase of solar cycle 23 while interval 2 (red shaded region) took place during the declining phase of the same solar cycle. The sunspot number prediction suggests that Juno is expected to arrive at Jupiter during the declining phase of solar cycle 24. These Ulysses observations can be used to provide a statistical baseline for the solar wind and interplanetary magnetic field (IMF) conditions expected at Jupiter during the upcoming Juno mission in 2016.
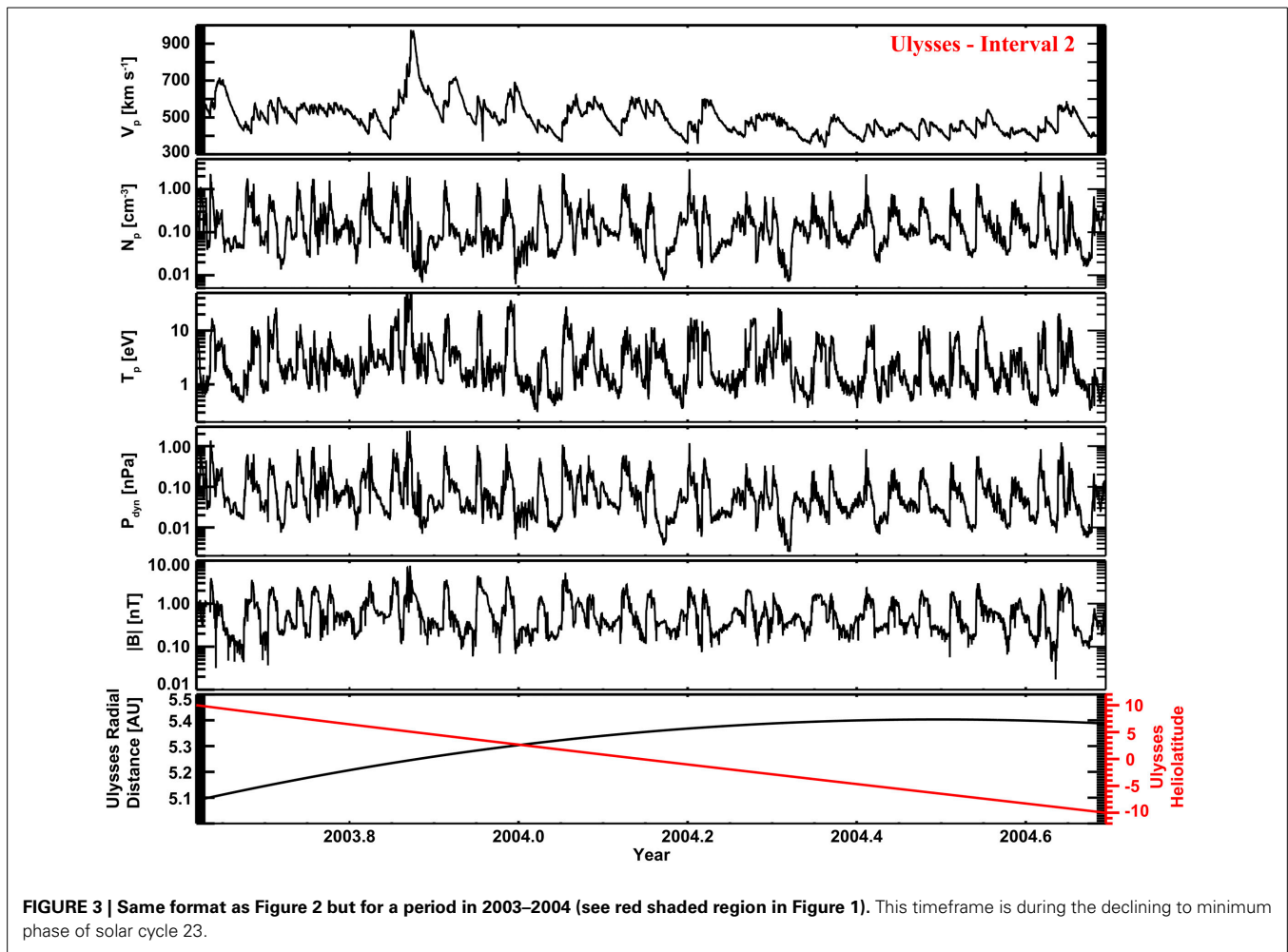
SOLAR WIND AT 5 AU

Figure 2 shows an overview of selected solar wind and IMF parameters, and the Ulysses spacecraft radial distance and heliolatitude from June 4, 1997 through July 8, 1998. This period, corresponding to interval 1 in **Table 1**, occurred during the rising to maximum phase of solar cycle 23. The top panel displays 1-h averages of the solar wind proton speed measured by Ulysses/SWOOPS. The solar wind during this period was relatively slow, ranging between ∼300 and 500 km s^{-1} except for two fast interplanetary coronal mass ejections (ICMEs) in April

and June, 1998. A total of 29 ICMEs were identified during this period (Ebert et al., 2009), most of them becoming entrained in the ambient solar wind by the time they reached 5 AU. The proton density and temperature, proton + alpha particle dynamic pressure, and IMF magnitude were all highly variable, each spanning nearly two orders or magnitude. McComas et al. (2014) demonstrated a bimodal distribution for the solar wind dynamic pressure observations during the ±4 day period upstream and downstream of the speed jumps associated with many of these ICMEs. The size and dynamics of the outer jovian magnetosphere were likely influenced by changes in the solar wind dynamic pressure associated with ICMEs observed at 5 AU during this timeframe.

Figure 3 shows an overview of selected solar wind and IMF parameters for the period from August 14, 2003 through September 11, 2004, corresponding to interval 2 in **Table 1**. This period occurred during the declining to minimum phase of solar cycle 23. There were 9 ICMEs identified during this period, roughly a third of the number observed during interval 1. The parameters shown here have a more ordered structure relative to those in **Figure 2** with successive peaks and valleys in their

FIGURE 2 | Solar wind plasma and interplanetary magnetic field (IMF) observations during a period in 1997–1998 when Ulysses was near 5 AU and within 10° of the ecliptic plane (see blue shaded region in Figure 1). This timeframe is during the rising to maximum phase of solar cycle 23. Shown here, from top to bottom, are the solar wind proton speed, density, and temperature, proton + alpha particle dynamic pressure, IMF magnitude, and Ulysses radial distance and heliolatitude.

FIGURE 3 | Same format as Figure 2 but for a period in 2003–2004 (see red shaded region in Figure 1). This timeframe is during the declining to minimum phase of solar cycle 23.
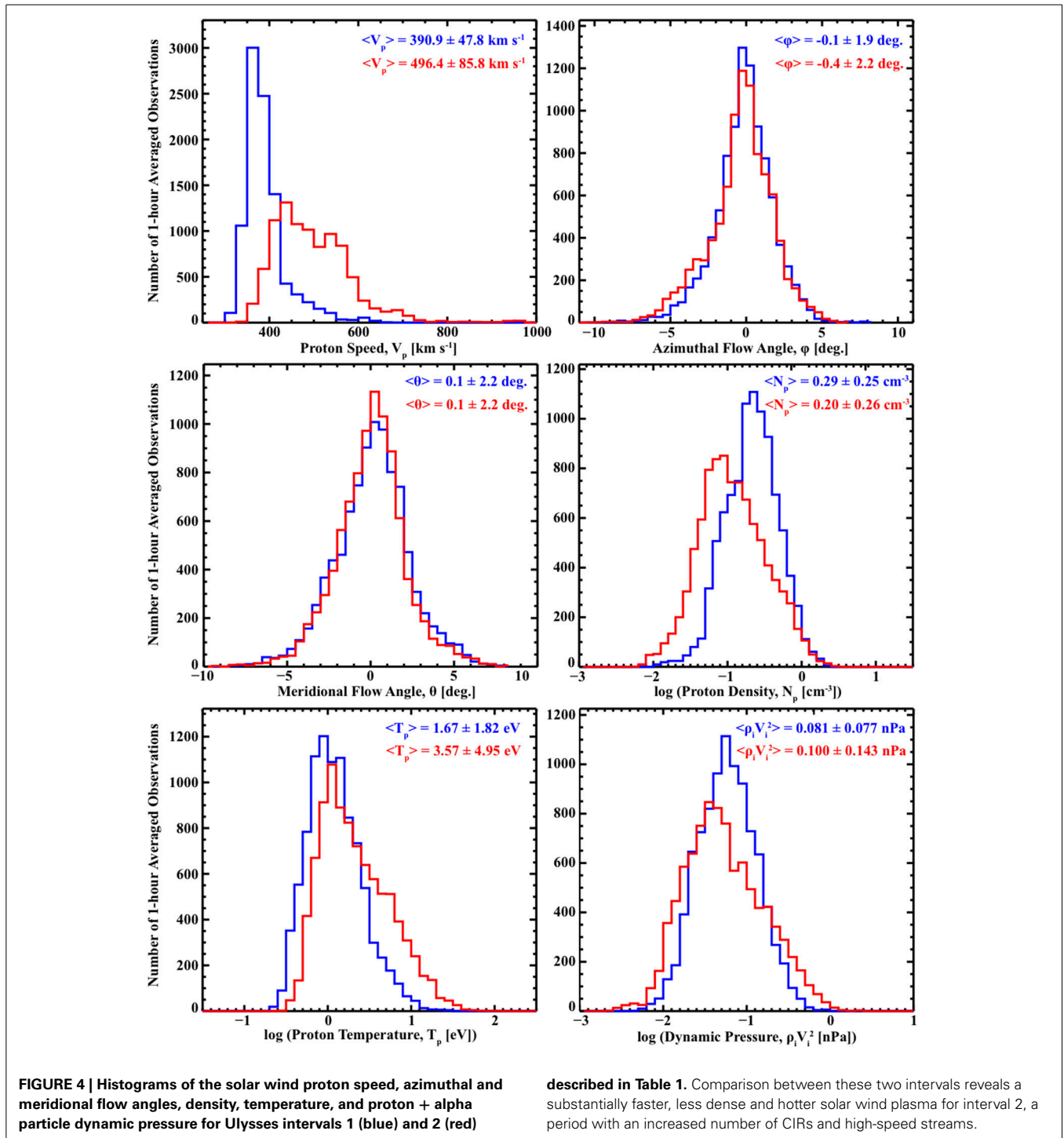
magnitudes that reoccur at roughly the solar rotation rate. This trend is representative of a solar wind structure composed of compressions and rarefactions that are typically associated with corotating interaction regions (CIRs) and high-speed streams. Here, the solar wind speed ranges between ~400 and 700 km s^{-1} with a brief excursion to ~925 km s^{-1} during the passage of a fast ICME in November 2003. These faster wind speeds can be attributed to the presence of high-speed streams that originated from fast wind producing low latitude coronal holes, including one that that persisted for most of 2003 (Elliott et al., 2012), and a couple of fast ICMEs (McComas et al., 2006). The solar wind and IMF parameters shown here also showed roughly two order of magnitude variations, typically with sharp increases in the solar wind compressions and more gradual declines in the rarefactions. Both the solar wind speed and dynamic pressure bounding the compressions and their associated speed jumps had bimodal distributions during this period (McComas et al., 2014) and the extent of the jovian magnetosphere was likely influenced by CIRs and high speed streams at 5 AU during this timeframe.

Figures 4, **5** show histograms of selected solar wind and IMF parameters for intervals 1 (blue) and 2 (red) to directly compare the solar wind and IMF during the rising to maximum and declining phases of solar cycle 23. The solar wind during
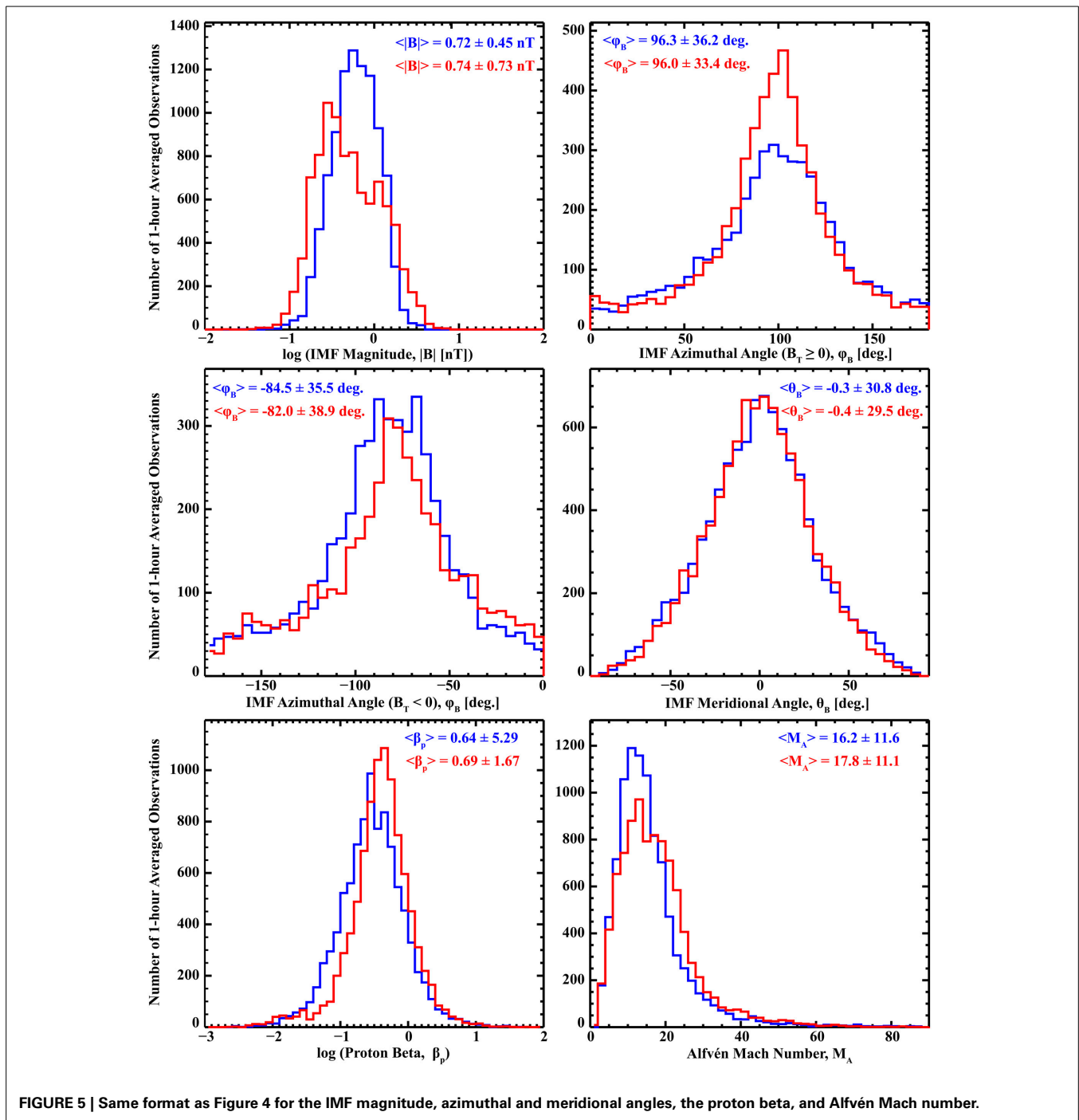
interval 1 is, on average, slower, cooler, and more dense while the distribution of these parameters had larger standard deviations for interval 2. The dynamic pressure mean and standard deviation were larger for interval 2 but not the median. These differences highlight how the solar wind properties at 5 AU can vary for solar wind composed mainly of slow wind and ICMEs (interval 1) vs. that composed primarily of CIRs and high-speed streams (interval 2). The solar wind flow angles are nearly identical during the two periods and show only small deviations from radial flow. The mean values for IMF magnitude are also similar ($|B|$~0.7 nT) although the distribution for interval 2 has a much larger standard deviation, $\sigma_{|B|} = 0.73$ nT, compared to $\sigma_{|B|} = 0.45$ nT for interval 1. The spiral (azimuthal) angle of the IMF is nearly tangential to the radial (Sun-Jupiter) direction while the IMF meridional angles have at $1-\sigma$ deviation of $\pm30°$ relative to Jupiter's north-south direction. The proton beta distribution means are $< \beta_p >_{interval1} = 0.64$ and $< \beta_p >_{interval2} = 0.69$, indicating that the magnetic pressure is, on average, larger than the proton thermal pressure during both periods. The solar wind flow at 5 AU is super-Alfvénic, the Alfvén Mach number having a mean and standard deviation of 16.2 ± 11.6 (interval 1) and 17.8 ± 11.1 (interval 2). These Mach numbers are more than double the average value at 1 AU (e.g., Lavraud and Borovsky, 2008)

FIGURE 4 | Histograms of the solar wind proton speed, azimuthal and meridional flow angles, density, temperature, and proton + alpha particle dynamic pressure for Ulysses intervals 1 (blue) and 2 (red) described in Table 1. Comparison between these two intervals reveals a substantially faster, less dense and hotter solar wind plasma for interval 2, a period with an increased number of CIRs and high-speed streams.

and strongly influence the strength and shape of Jupiter's bow shock (e.g., Slavin et al., 1985). Studies of reconnection on the dayside magnetopause suggest such high Mach numbers reduce the reconnection rate between the IMF and planetary magnetic field (Swisdak et al., 2003; Mozer and Hull, 2010; Phan et al., 2010; Desroche et al., 2012; Masters et al., 2012). Finally, we note that none of the distributions shown here are bimodal; it is only after the observations are separated by solar wind structure type that

the bimodal nature of the solar wind at 5 AU becomes apparent (Joy et al., 2002; McComas et al., 2014).

Tables 2, 3 show the statistical properties during these intervals for all solar wind and IMF parameters examined here. These values should serve as the baseline of any effort aimed at studying the influence of the solar wind on the dynamics of Jupiter's magnetosphere. Since some of the distributions are far from Gaussian, we include the median, 10th and 90th percentiles as well as the mean

FIGURE 5 | Same format as Figure 4 for the IMF magnitude, azimuthal and meridional angles, the proton beta, and Alfvén Mach number.

and standard deviation. The density, temperature, dynamic pressure, and proton beta particularly illustrate the effects of having distributions of high-valued tails that result in much larger mean over median values.

THE SIZE OF JUPITER'S MAGNETOSPHERE

The strength and location of a planetary bow shock are influenced by parameters such as the upstream solar wind Mach number and dynamic pressure, and the size and shape of the obstacle (e.g., Slavin et al., 1985; Farris and Russell, 1994). The
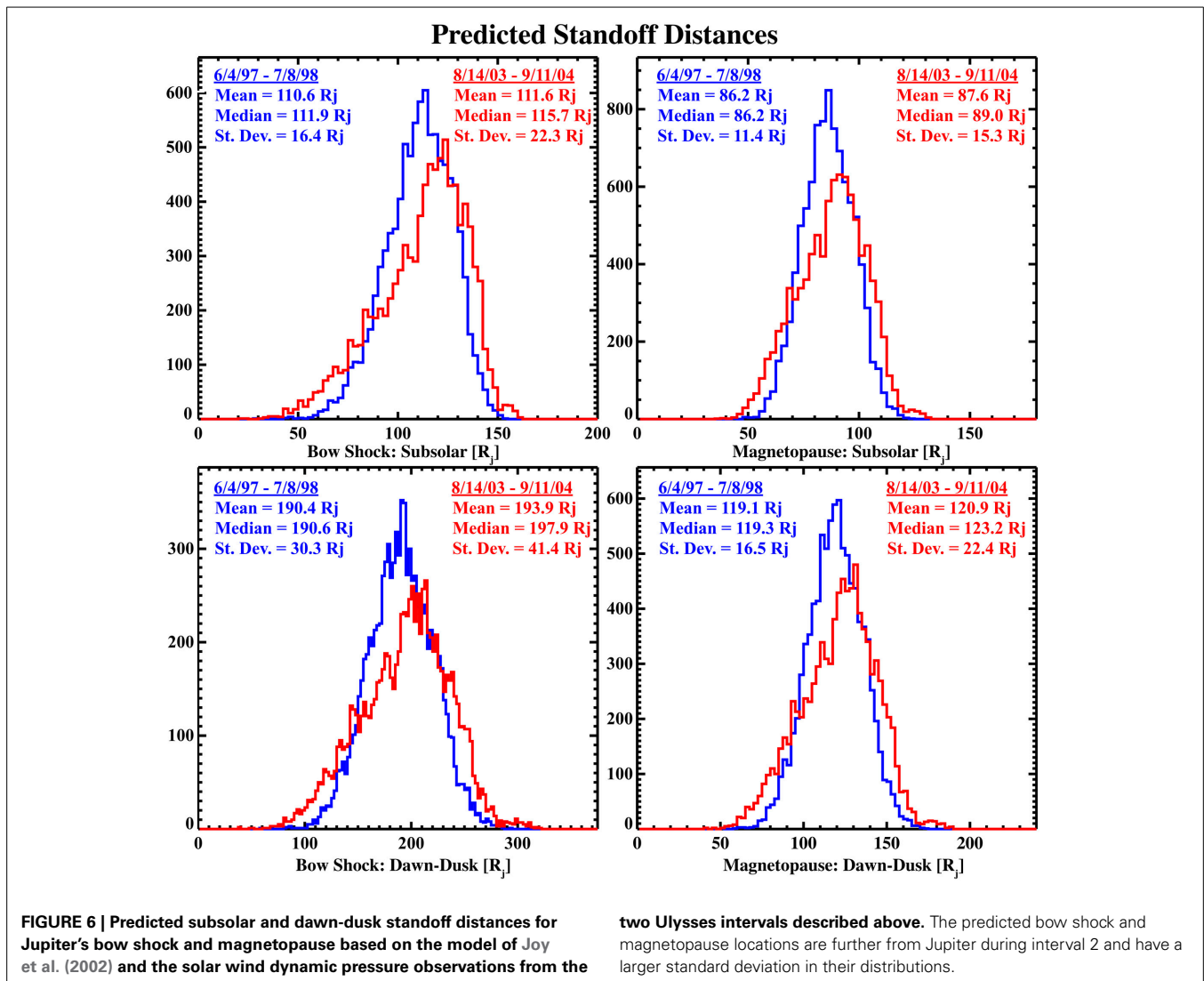
magnetopause standoff distance is a function of the pressure balance between the solar wind dynamic pressure (ρV^2) and the dominant internal pressure, typically magnetic and/or thermal, within the magnetosphere. At Earth, it is the magnetic pressure from the planet's roughly dipole magnetic field that stands off the solar wind and the dayside magnetopause standoff distance varies as the sixth root of ρV^2 (Chapman and Ferraro, 1930). At Jupiter, the pressure balance is mediated by the high beta (plasma pressure dominated) plasma sheet in the outer magnetosphere (Mauk et al., 2004), causing the location of the dayside

Table 2 | Statistics of 5 AU solar wind and IMF properties for Ulysses Interval 1.

Parameter	10th percentile	Mean	Median	Standard deviation	90th percentile
V_p [km s^{-1}]	346.8	390.9	378.7	47.8	449.1
V_α [km s^{-1}]	347.9	393.1	380.7	48.2	452.3
Azimuthal flow angle, φ [deg.]	−2.51	−0.15	−0.07	1.90	2.09
Meridional flow angle, θ [deg.]	−2.71	0.12	0.21	2.22	2.73
N_p [cm^{-3}]	0.07	0.29	0.22	0.25	0.60
N_α [cm^{-3}]	0.001	0.007	0.004	0.008	0.015
N_α/N_p [%]	0.80	2.51	2.16	1.61	4.70
T_p [eV]	0.49	1.67	1.13	1.82	3.22
Mass flux [kg m^{-2} s^{-1}] × 10^{-15}	0.05	0.21	0.15	0.18	0.42
$\rho_i V_i^2$ [nPa]	0.021	0.081	0.058	0.077	0.167
Energy flux [mW m^{-2}]	0.004	0.016	0.011	0.018	0.034
$N_p k T_p$ [pPa]	0.01	0.09	0.04	0.14	0.20
B_R [nT]	−0.382	−0.001	−0.002	0.338	0.367
B_T [nT]	−0.820	−0.023	−0.036	0.634	0.770
B_N [nT]	−0.468	0.002	0.001	0.450	0.464
$|B|$[nt]	0.26	0.72	0.60	0.45	1.32
IMF azimuthal angle, φ_B ($B_T \geq 0$) [deg.]	45.4	96.3	98.9	36.2	141.1
IMF azimuthal angle, φ_B ($B_T < 0$) [deg.]	−133.7	−84.5	−82.0	35.5	−41.4
IMF meridional angle, θ_B [deg.]	−40.5	−0.32	0.12	30.77	39.5
$B^2/2\mu_o$ [pPa]	0.03	0.29	0.15	0.41	0.67
β_p	0.073	0.64	0.29	5.29	1.08
M_A	6.9	16.2	13.9	11.6	26.6
ICME rate [#/day]	0.07				

Table 3 | Statistics of 5 AU solar wind and IMF properties for Ulysses Interval 2.

Parameter	10th percentile	Mean	Median	Standard deviation	90th percentile
V_p [km s^{-1}]	403.8	496.4	482.6	85.6	595.0
V_α [km s^{-1}]	407.0	499.9	486.9	85.6	599.5
Azimuthal flow angle, φ [deg.]	−3.30	−0.36	−0.16	2.15	2.09
Meridional flow angle, θ [deg.]	−2.57	0.059	0.12	2.15	2.45
N_p [cm^{-3}]	0.03	0.20	0.11	0.26	0.50
N_α [cm^{-3}]	0.001	0.007	0.004	0.011	0.017
N_α/N_p	1.55	3.69	3.67	1.74	5.51
T_p [eV]	0.72	3.57	1.82	4.94	8.15
Mass flux [kg m^{-2} s^{-1}] × 10^{-15}	0.030	0.194	0.101	0.256	0.477
$\rho_i V_i^2$ [nPa]	0.014	0.100	0.048	0.143	0.247
Energy flux [mW m^{-2}]	0.003	0.026	0.012	0.043	0.065
$N_p k T_p$ [pPa]	0.01	0.18	0.03	0.45	0.48
B_R [nT]	−0.368	−0.010	−0.006	0.369	0.342
B_T [nT]	−1.050	−0.017	0.088	0.836	0.813
B_N [nT]	−0.411	−0.008	−0.0003	0.495	0.389
$|B|$[nt]	0.177	0.743	0.468	0.728	1.695
IMF azimuthal angle ($B_T \geq 0$), φ_B [deg.]	52.0	96.0	98.6	33.4	135.5
IMF azimuthal angle ($B_T < 0$), φ_B [deg.]	−139.6	−82.0	−79.5	38.9	−31.6
IMF meridional angle, θ_B [deg.]	−39.5	−0.4	−0.1	29.5	37.4
$B^2/2\mu_o$ [pPa]	0.01	0.43	0.09	1.02	1.14
β_p	0.12	0.69	0.41	1.65	1.31
M_A	7.0	17.8	16.0	11.1	29.4
ICME rate [#/day]	0.02				

FIGURE 6 | Predicted subsolar and dawn-dusk standoff distances for Jupiter's bow shock and magnetopause based on the model of Joy et al. (2002) and the solar wind dynamic pressure observations from the **two Ulysses intervals described above.** The predicted bow shock and magnetopause locations are further from Jupiter during interval 2 and have a larger standard deviation in their distributions.

magnetopause to respond more strongly to changes in the solar wind dynamic pressure relative to Earth (Slavin et al., 1985; Huddleston et al., 1998; Joy et al., 2002; Alexeev and Belenkaya, 2005). Joy et al. (2002) used jovian boundary position observations from several spacecraft and magnetohydrodynamic (MHD) simulations to derive a three-dimensional model for Jupiter's magnetopause and bow shock. The shapes of these boundaries were expressed as second order polynomials with the coefficients being a function of the solar wind dynamic pressure. A Jupiter-centered coordinate system was used with the x-axis pointing toward the Sun, z being along Jupiter's spin axis, and y completing the right handed system with positive toward dusk. Results from this model showed the standoff distances of the magnetopause and bow shock (though with less statistical confidence) to have bimodal probability distributions. These distributions were interpreted as resulting from the bimodal distribution of solar wind parameters at 5 AU. There, the solar wind is typically composed of compression and rarefactions that exhibit a bimodal distribution in solar wind dynamic pressure, accounting for the bimodal

distribution of the jovian magnetosphere's size (e.g., McComas et al., 2014).

In this Section, we use the Joy et al. (2002) model and the solar wind dynamic pressure observations from intervals 1 and 2 to examine the predicted bow shock and magnetopause locations at Jupiter for two different periods in solar cycle 23. **Figure 6** shows the distribution of predicted subsolar and dawn-dusk standoff distances for the bow shock and magnetopause, along with their mean, median, and standard deviation, for the two intervals studied here. The calculated mean subsolar and dawn-dusk standoff distances for the bow shock were 110.6 ± 16.4 R_J and 190.4 ± 30.3 R_J for interval 1 and 111.6 ± 22.3 R_J and 193.9 ± 41.4 R_J for interval 2. The calculated mean magnetopause standoff distances were 86.2 ± 11.4 R_J and 119.1 ± 16.5 R_J for interval 1 and 87.6 ± 15.3 R_J and 120.9 ± 22.4 R_J for interval 2. These predictions suggest that the bow shock and magnetopause were, on average, further upstream of Jupiter during the declining phase of solar cycle 23, consistent with the smaller median for the solar wind dynamic pressure during interval 2. The larger excursions
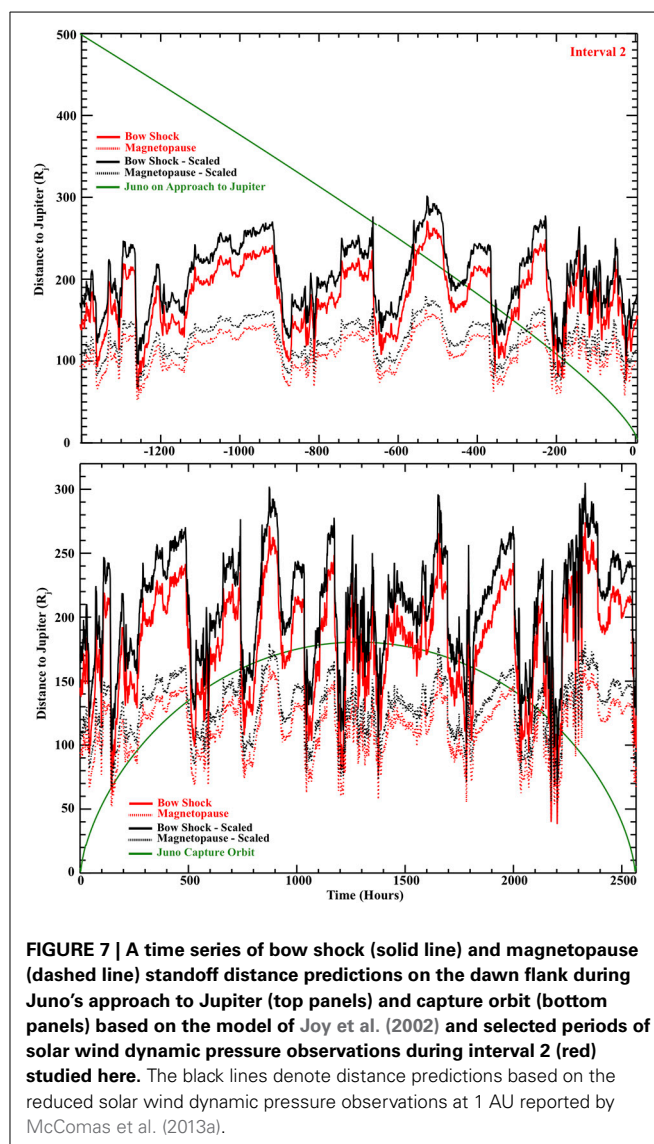
predicted for these boundaries during interval 2 results from the broader distribution of solar wind dynamic pressures during that timeframe. Interestingly, the expected bimodal nature of these standoff distance distributions is not apparent here and the predictions favor a magnetosphere in a more expanded state. This may be due to the presence of intermediate speed solar wind with dynamic pressure distributions that are not bimodal or, perhaps, because Jupiter's magnetosphere does not immediately respond to changes in the solar wind dynamic pressure (e.g., McComas et al., 2014).

IMPLICATIONS FOR JUNO

In 2016, the Juno mission (Bolton and the Juno Science Team, 2010) is scheduled to become the ninth spacecraft, and second orbiter, to explore Jupiter's magnetosphere and the first to explore its polar regions. Approaching the planet on the dawn flank, Juno will be inserted into a polar orbit in July 2016, and embark on a 107-day capture orbit (apojove of ∼180 Rj near the dawn flank) followed by a series of thirty 11-day polar orbits with an apojove of ∼38 Rj and a perijove of ∼1.05 Rj (Bagenal et al., 2014). During its approach, Juno is expected spend ∼10–15 days in the regions bounding the dawn side of Jupiter's magnetosphere, providing an unprecedented opportunity to study the solar wind interaction along Jupiter's dawn magnetosphere and investigate the dynamics of the outer magnetosphere in that region (Bagenal et al., 2014). For the currently planned 107-day capture orbit and using the Joy et al. (2002) model and solar wind dynamic pressure observations at 5 AU from Ulysses during a period similar to interval 2 studied here, Bagenal et al. (2014) predicted that Juno would cross Jupiter's bow shock and magnetopause 64 ± 9 times and 42 ± 9 times, respectively. These predictions did not account the long-term declining trend in the solar wind dynamic pressure reported by McComas et al. (2013a) that will likely result in a more extended magnetosphere in 2016 than predicted from Ulysses observations in 2003–2004.

Figure 7 shows a time series of bow shock and magnetopause standoff distances on the dawn side of Jupiter's magnetosphere for a period equivalent to Juno's approach phase (top panel) and capture obit (bottom panel). These values were calculated using Joy et al. (2002) for the case of $x = z = 0$ and a time series of solar wind dynamic pressure observations during interval 2. We also show these distances scaled by the reduction in solar wind dynamic pressure at 1 AU reported by McComas et al. (2013a). The dynamic pressure observations were scaled by the mean of the dynamic pressure observations during the current "mini" solar maximum (see Table 1 from McComas et al., 2013a) scaled to 5.2 AU divided by the mean of the solar wind dynamic pressures for intervals 1 and 2, respectively [scaling factor $= < \rho V^2 >_{\text{"mini max"}}$ $\times \left(\frac{1 AU}{5.2 AU}\right)^2 / < \rho V^2 >_{\text{Ulysses interval 1,2}}$]. **Table 4** shows statistical properties for the bow shock and magnetopause distance estimates during interval 2, including their scaled values. As expected, the reduction in solar wind dynamic pressure resulted in a prediction supporting a more expanded jovian magnetosphere during the Juno mission timeframe (2016–2017) than predicted from Ulysses observations in 2003–2004.

We revised the Bagenal et al. (2014) estimate of the number of boundary crossings during Juno's capture orbit to reflect these

FIGURE 7 | A time series of bow shock (solid line) and magnetopause (dashed line) standoff distance predictions on the dawn flank during Juno's approach to Jupiter (top panels) and capture orbit (bottom panels) based on the model of Joy et al. (2002) and selected periods of solar wind dynamic pressure observations during interval 2 (red) studied here. The black lines denote distance predictions based on the reduced solar wind dynamic pressure observations at 1 AU reported by McComas et al. (2013a).

changes in dynamic pressure. We predict that the spacecraft will cross Jupiter's bow shock and magnetopause 45 ± 13 and 55 ± 14 times, respectively, for solar wind similar to interval 2. If these approximations prove to be accurate, Juno will likely spend less time in the regions bounding the dawn side of Jupiter's magnetosphere during its capture orbit than initially predicted. On the other hand, the weaker solar wind dynamic pressure and more extended magnetosphere mean that the Juno spacecraft will likely encounter these boundaries sooner on approach to Jupiter, with a 10% probability of crossing the bow shock and magnetopause as early as June 6, 2016 at 273 Rj and June 20, 2016 at 164 Rj, respectively.

The prime science phase of the mission is expected to being on October 19, 2016 where Juno will spend a year exploring the polar regions of Jupiter's magnetosphere through a series of highly eccentric shorter period (currently planned to be 11 days) orbits. During the polar orbits, Juno will be confined to the inner and middle regions of the magnetosphere. At high latitudes, Juno

Table 4 | Statistics of predicted jovian bow shock and magnetopause crossing distances for Ulysses interval 2.

Parameter	10th percentile	Mean	Median	Standard deviation	90th percentile
BS: Subsolar	79.3	111.6	115.7	22.3	137.3
BS: Dawn–Dusk	136.5	193.9	197.9	41.4	244.7
BS: Subsolar (Scaled)	96.0	124.9	128.8	20.0	147.7
BS: Dawn–Dusk (Scaled)	163.1	221.2	224.6	42.1	273.7
MP: Subsolar	66.0	87.5	89.0	15.3	106.6
MP: Dawn–Dusk	89.6	120.9	123.2	22.4	148.4
MP: Subsolar (Scaled)	75.7	97.6	99.2	15.5	116.8
MP: Dawn–Dusk (Scaled)	104.3	135.7	137.6	22.8	164.0

BS, Bow shock; MP, magnetopause.

will directly observe auroral phenomena and may or may not cross magnetic field lines that are open to the solar wind. It will be important to have knowledge of the solar wind conditions upstream of the planet during these times to untangle the dynamics caused by internal processes vs. those initiated by external stresses imposed on the magnetosphere. Unfortunately, similar to previous missions, there will be no solar wind monitor upstream of Jupiter at these times. Instead, the Juno team will have to rely on observations from NASA's network of 1 AU spacecraft along with modeling of the solar wind propagation to 5.2 AU (e.g., Zieger and Hansen, 2008).

The validated 1-D MHD model of Zieger and Hansen (2008) has been used to propagate the solar wind from 1 AU to Jupiter (Clarke et al., 2009) and Saturn (Zieger et al., 2010). Their model works best during periods of recurring solar wind speed such as the declining phase of the solar cycle and the best predictions were made within ±75 days of apparent opposition. The solar wind speed prediction was found to have the highest accuracy, followed by the IMF magnitude and solar wind density. The shock arrival times were predicted to within 10–15 h during the declining phase and the predictions were less accurate during solar maximum. Given that Juno is expected to explore Jupiter's magnetosphere during the declining phase of solar cycle 24 (see **Figure 1**), this model might be appropriate for predicting the solar wind conditions upstream of Jupiter during that time.

Juno's distance from Jupiter during its capture orbit and science orbits is plotted in **Figure 8**. Superimposed on the plot are periods when 1 AU spacecraft ACE (Stone et al., 1998), Wind (Acuña et al., 1995), and STEREO-A and -B (Kaiser et al., 2008), each equipped with instruments to measure the solar wind plasma and IMF, are within ±75 days from apparent opposition with Jupiter. Jupiter will be in good alignment with at least one of these 1 AU spacecraft throughout most of the Juno mission. There will be periods where two 1 AU spacecraft straddle Jupiter's longitude at the same time and any model will need to account for the solar wind at both locations before propagating the solar wind to 5 AU, providing an important second constraint for predicting the solar wind conditions upstream of Jupiter.
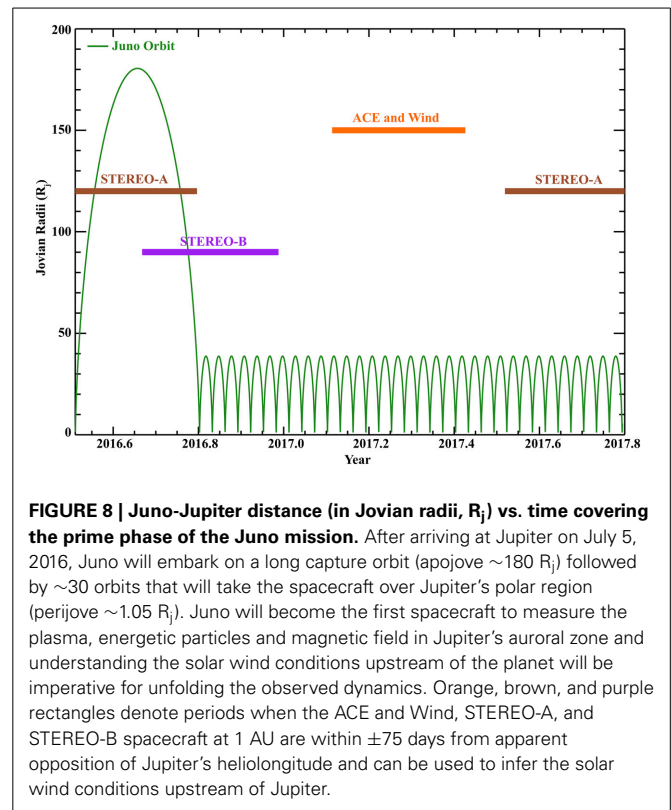

FIGURE 8 | Juno-Jupiter distance (in Jovian radii, R_J) vs. time covering the prime phase of the Juno mission. After arriving at Jupiter on July 5, 2016, Juno will embark on a long capture orbit (apojove ∼180 R_J) followed by ∼30 orbits that will take the spacecraft over Jupiter's polar region (perijove ∼1.05 R_J). Juno will become the first spacecraft to measure the plasma, energetic particles and magnetic field in Jupiter's auroral zone and understanding the solar wind conditions upstream of the planet will be imperative for unfolding the observed dynamics. Orange, brown, and purple rectangles denote periods when the ACE and Wind, STEREO-A, and STEREO-B spacecraft at 1 AU are within ±75 days from apparent opposition of Jupiter's heliolongitude and can be used to infer the solar wind conditions upstream of Jupiter.

DISCUSSION

The role of the solar wind in shaping the topology of and controlling the dynamics within Jupiter's magnetosphere is an open issue (e.g., Krupp et al., 2004) that remains under considerable debate (Cowley et al., 2008; McComas and Bagenal, 2008). Here, we examined Ulysses solar wind and IMF observations at 5 AU during the rising and declining phases of solar cycle 23 and the predicted response of the jovian magnetosphere during these times. We then used these results to estimate the solar wind and IMF conditions upstream of Jupiter and the expected size of the jovian magnetosphere during the Juno mission. Sunspot number predictions based on the methods described in Hathaway et al. (1994) suggest that Juno's arrival at Jupiter in 2016 will coincide with the declining phase of solar cycle 24.

The solar wind in the declining phase was composed primarily of CIRs and high-speed streams and was, on average, faster, hotter, less dense, and more Alfvénic relative to the solar wind during the rising phase, composed mainly of slow wind and ICMEs. Several of the solar wind and IMF properties studied here had extended, non-Gaussian tails in their distributions that resulted in large standard deviations and much larger mean over median values. Interestingly, none of the solar wind distributions reported here were bimodal, a feature that was used to explain the reported bimodal distribution in bow shock and magnetopause standoff distances at Jupiter (Joy et al., 2002). This may be due to the presence of intermediate speed solar wind not associated with ICMEs, CIRs, and high-speed streams having distributions that are not bimodal; it is only after the observations are separated by solar wind structure type that the

bimodal nature of the solar wind at 5 AU becomes apparent (Joy et al., 2002; McComas et al., 2014).

We used the Ulysses solar wind dynamic pressure observations at 5 AU along with the Joy et al. (2002) model to predict the subsolar and dawn-dusk bow shock and magnetopause stand-off distances at Jupiter during the two periods described above. The mean and median of the predicted standoff distances were larger during the declining phase of solar cycle 23 but only by ∼1–4%. The standard deviation of these parameters was also larger, consistent with the larger standard deviation for the solar wind dynamic pressures during this timeframe. Surprisingly, the bimodal distribution for the bow shock and magnetopause stand-off distances was not observed, and the predictions implied a magnetosphere in a more expanded state. While McComas et al. (2014) showed bimodal solar wind speed and dynamic pressure distributions in the days bounding the ICMEs (rising phase) and CIR compressions (descending phase) during the two intervals studied here, there was also a large fraction (∼50% of the observations) of solar wind during these times with dynamic pressure distributions that were not bimodal. These distributions may have washed out the bimodal structure of the bow shock and magnetopause distributions. These authors also proposed several time constants for the multi-step process associated with the response of the magnetosphere to changes in solar wind dynamic pressure. They suggested that the compression of the magnetosphere is expected to lag the initial rise in dynamic pressure by several hours due to the time required for the pressure pulse to be transmitted through the magnetosphere and the shedding of plasma from the plasma disk. The expansion of the magnetosphere back to a relaxed state is constrained by the several days decline in solar wind dynamic pressure during a solar wind rarefaction. Joy et al. (2002) is a static model that does not account for these time lags and this may be why the predicted standoff distance distributions are not bimodal during the periods studied here.

We also made predictions for the extent of the magnetosphere and the number of bow shock and magnetopause crossings expected during Juno's approach to Jupiter and capture orbit by accounting for the decades long decline in solar wind dynamic pressure reported by McComas et al. (2013a). Our calculations suggest that Jupiter's bow shock and magnetopause will, on average, be at least 8–12% further from Jupiter for the Juno mission than during the 1997–2004 Ulysses era, if these trends continue. The estimated number of bow shock and magnetopause crossings during Juno's capture orbit, based on solar wind dynamic pressure observations from interval 2, have been changed by −30 and 31%, respectively, compared to initial predictions (Bagenal et al., 2014). These revised predictions reflect a more extended magnetosphere where Juno will spend less time in the upstream solar wind and more time in the magnetosheath and magnetosphere. That being said, the weaker solar wind dynamic pressure should provide the Juno spacecraft an opportunity to encounter these boundaries sooner on approach to Jupiter, with a 10% probability of crossing the bow shock and magnetopause as early as ∼30 and ∼15 days, respectively, prior to its scheduled arrival.

In addition to the long-term reduction in solar wind dynamic pressure, McComas et al. (2013a) also reported on similar trends for several other solar wind fluid properties including its speed, temperature, and thermal pressure, and the IMF magnitude and plasma beta. Coupled with the higher Mach number values generally observed in the plasma upstream of Jupiter relative to Earth, these trends will have significant implications for the solar wind-Jupiter interaction during the Juno timeframe. The focus will be to investigate mechanisms that lead to coupling of the IMF to Jupiter's magnetic field and solar wind entry into the magnetosphere along the dawn flank. Two competing theories are (i) large scale reconnection on the dayside that is closed in the tail, followed by a return flow along the dawn side (e.g., Cowley et al., 2003) and (ii) interactions at the magnetospheric boundary, either by the opening and reclosing of the IMF and planetary magnetic field along the magnetopause (McComas and Bagenal, 2007) or stresses imposed by viscous interactions between magnetospheric and solar wind plasma (e.g., Delamere and Bagenal, 2010). Two key solar wind parameters that are likely to influence this type of interaction at Jupiter are the Mach number and plasma beta (e.g., Jackman and Arridge, 2011). It has recently been shown that the reconnection rate is strongly influenced by the plasma beta difference between the magnetosheath and magnetopause (e.g., Phan et al., 2010), the magnetosheath beta being strongly influenced by the upstream solar wind Mach number and plasma beta and the cone angle of the IMF (Scurry et al., 1994). It will be interesting to see how the long-term changes in solar wind and IMF properties at 1 AU influence this interaction during the Juno mission.

Juno is equipped with instruments to make *in situ* measurements of the ions and electrons (JADE; McComas et al., 2013b), energetic particles (JEDI; Mauk et al., 2014), magnetic fields (MAG; Connerney et al., in preparation) and plasma waves (Waves; Kurth et al., in preparation) in Jupiter's magnetosphere. These instruments are expected to directly measure these properties in the solar wind and magnetosheath during Juno's approach to Jupiter and capture orbit. These observations, in coordination with remote sensing measurements from instruments both on the spacecraft and at Earth, will provide a prime opportunity to study the solar wind-magnetosphere interaction at Jupiter. Unfortunately, we will not have direct measurement of the solar wind conditions upstream of Jupiter during Juno's prime mission polar orbits, measurements that could prove critical for untangling the dynamics caused by internal processes vs. those initiated by external stresses imposed on the magnetosphere. Instead, the solar wind conditions upstream of the planet will have to be inferred from observations at 1 AU that are propagated to ∼5.2 AU using analytical calculations and/or models. Fortunately, there will be good alignment between Jupiter and at least one 1 AU spacecraft for most of the mission and a significant period of time with two spacecraft. A significant effort should be made to validate these solar wind propagation methods during the approach and capture orbit phases prior to Juno entering into polar orbit around Jupiter.

To conclude, while this study is aimed at supporting investigations of solar wind-magnetosphere interactions at Jupiter, including during several upcoming missions, much of the open questions related to topic could be addressed by having a solar wind monitor upstream of Jupiter during these mission timeframes.

While this may have not been feasible in the past due to constrained resources, the recent emergence of small satellites (e.g., cubesats) may provide a low cost option to maximize the science return on these large class missions.

ACKNOWLEDGMENTS

REFERENCES

Acúna, M. H., Oglivie, K. W., Curtis, D. N., Fairfield, S. A., and Mish, W. H. (1995). The global geospace science program and its investigations. *Space Sci. Rev.* 71, 5.

Alexeev, I. I., and Belenkaya, E. S. (2005). Modeling of the jovian magnetosphere. *Ann. Geophys.* 23, 809–826. doi: 10.5194/angeo-23-809-2005

Bagenal, F., Adriani, A., Allegrini, F., Bolton, S. J., Bonfond, B., Bunce, E. J., et al. (2014). Magnetospheric science objectives of the Juno mission. *Space Sci. Rev.* doi: 10.1007/s11214-014-0036-8. [Epub ahead of print].

Bagenal, F., Dowling, T., and McKinnon, W. (eds.). (2004). *Jupiter: Planet, Satellites, Magnetosphere.* Cambridge University Press.

Balogh, A., Beek, T. J., Forsyth, R. J., Hedgecock, P. C., Marquedant, R. J., Smith, E. J., et al. (1992). The magnetic field investigation on the ULYSSES mission—instrumentation and preliminary scientific results. *Astron. Astrophys. Suppl. Ser.* 92, 221.

Bame, S. J., Barraclough, B. L., Feldman, W. C., Gisler, G. R., Gosling, J. T., McComas, D. J., et al. (1992a). Jupiter's magnetosphere. *Science* 257, 1539.

Bame, S. J., McComas, D. J., Barraclough, B. L., Phillips, J. L., Sofaly, K. J., Chavez, J. C., et al. (1992b). The ulysses solar wind plasma experiment. *Astron. Astrophys. Suppl. Ser.* 92, 237–265.

Bolton, S. J., and the Juno Science Team. (2010). "The Juno mission," in *Proceedings IAU Symposium No. 269,*" eds C. Barbieri, S. Chakrabarti, M. Coradini, and M. Lazzarin (Padova: International Astronomical Union).

Bridge, H. S., Belcher, J. W., Lazarus, A. J., Sullivan, J. D., Bagenal, F., McNutt, R. L. Jr., et al. (1979b). Plasma observations near Jupiter—initial results from Voyager 2. *Science* 206:972. doi: 10.1126/science.206.4421.972

Bridge, H. S., Belcher, J. W., Lazarus, A. J., Sullivan, J. D., McNutt, R. L., Bagenal, F., et al. (1979a). Plasma observations near Jupiter—initial results from Voyager 1. *Science* 204:987. doi: 10.1126/science.204.4396.987

Chapman, S., and Ferraro, V. C. A. (1930). A new theory of magnetic storms. *Nature* 126, 129. doi: 10.1038/126129a0

Clarke, J. T., Nichols, J., Gérard, J.-C., Grodent, D., Hansen, K. C., Kurth, W., et al. (2009). Response of Jupiter's and Saturn's auroral activity to the solar wind. *J. Geophys. Res.* 114, A05210. doi: 10.1029/2008JA013694

Cowley, S. W. H., Badman, S. V., Imber, S. M., and Milan, S. E. (2008). Comment on "Jupiter: a fundamentally different magnetospheric interaction with the solar wind" by D. J. McComas, and F. Bagenal. *Geophys. Res. Lett.* 35, L10101. doi: 10.1029/2007GL032645

Cowley, S. W. H., Bunce, E. J., Stallard, T. S., and Miller, S. (2003). Jupiter's polar ionospheric flows: theoretical interpretation. *Geophys. Res. Lett.* 30, CiteID 1220. doi: 10.1029/2002GL016030

Delamere, P. A., and Bagenal, F. (2010). Solar wind interaction with Jupiter's magnetosphere. *J. Geophys. Res.* 115, A10201. doi: 10.1029/2010JA015347

Desroche, M., Bagenal, F., Delamere, P. A., and Erkaev, N. (2012). Conditions at the expanded Jovian magnetopause and implications for the solar wind interaction. *J. Geophys. Res.* 117, A07202. doi: 10.1029/2012JA017621

Dougherty, M. K. (2013). "JUICE: A European mission to Jupiter and its icy moons," in *American Geophysical Union, Fall Meeting 2013* (San Francisco, CA), Abstract #SM13D-03.

Ebert, R. W., McComas, D. J., Elliott, H. A., Forsyth, R. J., and Gosling, J. T. (2009). Bulk properties of the slow and fast solar wind and interplanetary coronal mass ejections measured by Ulysses: three polar orbits of observations. *J. Geophys. Res.* 114, A01109. doi: 10.1029/2008JA013631

Elliott, H. A., Henney, C. J., McComas, D. J., Smith, C. W., and Vasquez, B. J. (2012). Temporal and radial variation of the solar wind temperature-speed relationship. *J. Geophys. Res.* 117, A09102. doi: 10.1029/2011JA017125

Farris, M. H., and Russell, C. T. (1994). Determining the standoff distance of the bow shock: mach number dependence and use of models. *J. Geophys. Res.* 99, 17681. doi: 10.1029/94JA01020

Grodent, D., Clarke, J. T., Kim, J., Waite, J. H. Jr., Gérard, J.-C., and Kim, J. (2003). Jupiter's polar auroral emissions. *J. Geophys. Res.* 108, 1366. doi: 10.1029/2003JA010017

Gurnett, D. A., Kurth, W. S., Hospodarsky, G. B., Persoon, A. M., Zarka, P., Lecacheux, A., et al. (2002). Control of Jupiter's radio emission and aurorae by the solar wind. *Nature* 415, 985. doi: 10.1038/415985a

Hathaway, D. H., Wilson, R. M., and Reichmann, E. J. (1994). The shape of the solar cycle. *Solar Phys.* 151, 177. doi: 10.1007/BF00654090

Huddleston, D. E., Russell, C. T., Kivelson, M. G., Khurana, K. K., and Bennett, L. (1998). Location and shape of the Jovian magnetopause and bow shock. *J. Geophys. Res.* 103, 20075–20082. doi: 10.1029/98JE00394

Jackman, C. M., and Arridge, C. S. (2011). Solar cycle effects on the dynamics of Jupiter's and Saturn's magnetosphere. *Solar Phys.* 274, 481. doi: 10.1007/s11207-011-9748-z

Joy, S. P., Kivelson, M. G., Walker, R. J., Khurana, K. K., Russell, C. T., and Ogino, T. (2002). Probabilistic models of the Jovian magnetopause and bow shock locations. *J. Geophys. Res.* 107, SMP 17-1, CiteID 1309. doi: 10.1029/2001JA009146

Kaiser, M. L., Kucera, T. A., Davila, J. M., St. Cyr, O. C., Guhathakurta, M., and Christian, E. (2008). The STEREO mission: an introduction. *Space Sci. Rev.* 136, 5. doi: 10.1007/s11214-007-9277-0

Khurana, K. K., Kivelson, M. G., Vasyliunas, V. M., Krupp, N., Woch, J., Lagg, A., et al. (2004). "The configuration of Jupiter's magnetosphere," in *Jupiter: Planet, Satellites, Magnetosphere*, eds F. Bagenal, T. E. Dowling, and W. B. McKinnon (Cambridge: University Press), 593–616.

Kivelson, M. G., Khurana, K. K., Russell, C. T., and Walker, R. J. (1997). Intermittent short-duration magnetic field anomalies in the Io torus: evidence for plasma interchange? *Geophys. Res. Lett.* 24, 2127.

Kronberg, E. A., Woch, J., Krupp, N., Lagg, A., Khurana, K. K., and Glassmeier, K.-H. (2005). Mass release at Jupiter: substorm-like processes in the Jovian magnetotail. *J. Geophys. Res.* 110, A03211. doi: 10.1029/2004JA010777

Krupp, N., Vasyliunas, V. M., Woch, J., Lagg, A., Khurana, K. K., Kivelson, M. G., et al. (2004). "Dynamics of the Jovian magnetosphere," in *Jupiter: Planet, Satellites, Magnetosphere*, eds F. Bagenal, T. E. Dowling, and W. B. McKinnon (Cambridge: University Press), 617–638.

Kurth, W. S., Gurnett, D. A., Hospodarsky, G. B., Farrell, W. M., Roux, A., Dougherty, M. K., et al. (2002). The dusk flank of Jupiter's magnetosphere. *Nature* 415, 991. doi: 10.1038/415991a

Lavraud, B., and Borovsky, J. E. (2008). Altered solar wind-magnetosphere interaction at low Mach numbers: coronal mass ejections. *J. Geophys. Res.* 113, A00B08. doi: 10.1029/2008JA013192

Masters, A., Eastwood, J. P., Swisdak, M., Thomsen, M. F., Russell, C. T., Sergis, N., et al. (2012). The importance of plasma β conditions for magnetic reconnection at Saturn's magnetopause. *Geophys. Res. Lett.* 39, L08103. doi: 10.1029/2012GL051372

Mauk, B. H., Haggerty, D. K., Jaskulek, S. E., Schlemn, C. E., Brown, L. E., Cooper, S. A., et al. (2014). The Jupiter Energetic Particle Detector Instrument (JEDI) investigation for the Juno mission. *Space Sci. Rev.* doi: 10.1007/s11214-013-0025-3. [Epub ahead of print].

Mauk, B. H., McEntire, R. W., Williams, D. J., Lagg, A., Roelof, E. C., Krimigis, S. M., et al. (1998). Galileo-measured depletion of near-Io hot ring current plasmas since the Voyager epoch. *J. Geophys. Res.* 103, 4715–4722. doi: 10.1029/97JA02343

Mauk, B. H., Mitchell, D. G., McEntire, R. W., Paranicas, C. P., Roelof, E. C., Williams, D. J., et al. (2004). Energetic ion characteristics and neutral gas interactions in Jupiter's magnetosphere. *J. Geophys. Res.* 109, 9. doi: 10.1029/2003JA010270

McComas, D. J., Alexander, N., Allegrini, F., Bagenal, F., Beebe, C., Clark, G., et al. (2013b). The Jovian Auroral Distributions Experiment (JADE) on the Juno mission to Jupiter. *Space Sci. Rev.* doi: 10.1007/s11214-013-9990-9. [Epub ahead of print].

McComas, D. J., Angold, N., Elliott, H. A., Livadiotis, G., Schwadron, N. A., Skoug, R. M., et al. (2013a). Weakest solar wind of the space age and the current "mini" solar maximum. *Astrophys. J.* 779:2. doi: 10.1088/0004-637X/779/1/2

McComas, D. J., and Bagenal, F. (2007). Jupiter: a fundamentally different magnetospheric interaction with the solar wind. *Geophys. Res. Lett.* 34, L20106. doi: 10.1029/2007GL031078

McComas, D. J., and Bagenal, F. (2008). Re: Jupiter: a fundamentally different magnetospheric interaction with the solar wind, response to comment. *Geophys. Res. Lett.* 35, L10103. doi: 10.1029/2008GL034351

McComas, D. J., Bagenal, F., and Ebert, R. W. (2014). Bimodal size of Jupiter's magnetosphere. *J. Geophys. Res.* 119, 1523–1529. doi: 10.1002/2013JA019660

McComas, D. J., Elliott, H. A., Gosling, J. T., and Skoug, R. M. (2006). Ulysses observations of very different heliospheric structure during the declining phase of solar activity cycle 23. *Geophys. Res. Lett.* 33, L09102. doi: 10.1029/2006GL025915

Mozer, F. S., and Hull, A. (2010). Scaling the energy conversion rate from magnetic field reconnection to different bodies. *Phys. Plasmas* 17, 102906. doi: 10.1063/1.3504224

Pappalardo, R. T., Senske, D., Prockter, L., Paczkowski, B., Vance, S., Patterson, W., et al. (2013). "Science of the Europa clipper mission concept, American astronomical society," in *DPS Meetinging* (Denver), #45, #418.07.

Phan, T. D., Gosling, J. T., Paschmann, G., Pasma, C., Drake, J. F., Øiersoet, M., et al. (2010). The dependence of magnetic reconnection on plasma β and magnetic shear: evidence from solar wind observations. *Astrophys. J.* 719:L199. doi: 10.1088/2041-8205/719/2/L199

Scurry, L., Russell, C. T., and Gosling, J. T. (1994). Geomagnetic activity and the beta dependence of the dayside reconnection rate. *J. Geophys. Res.* 99, 14811. doi: 10.1029/94JA00794

Slavin, J. A., Smith, E. J., Spreiter, J. R., and Stahara, S. S. (1985). Solar wind flow about the outer planets: gas dynamic modeling of the Jupiter and Saturn bow shocks. *J. Geophys. Res.* 90, 6275–6286. doi: 10.1029/JA090iA07p06275

Smith, E. J., Fillius, R. W., and Wolfe, J. H. (1978). Compression of Jupiter's magnetosphere by the solar wind. *J. Geophys. Res.* 83, 4733. doi: 10.1029/JA083iA10p04733

Stahara, S. S., Rachiele, R. R., Spreiter, J. R., and Slavin, J. A. (1989). A three dimensional gasdynamic model for solar wind flow past nonaxisymmetric magnetospheres—application to Jupiter and Saturn. *J. Geophys. Res.* 94:13353. doi: 10.1029/JA094iA10p13353

Stone, E. C., Frandsen, A. M., Mewaldt, R. A., Christian, E. R., Margolies, D., Ornes, J. F., et al. (1998). The advanced composition explorer. *Space Sci. Rev.* 86:1.

Swisdak, M., Rogers, B. N., Drake, J. F., and Shay, M. A. (2003). Diamagnetic suppression of component magnetic reconnection at the magnetopause. *J. Geophys. Res.* 108, 1218. doi: 10.1029/2002JA009726

Walker, R. J., Ogino, T., and Kivelson, M. G. (2001). Magnetohydrodynamic simulations of the effects of the solar wind on the Jovian magnetosphere. *Planet Space Sci.* 49, 237. doi: 10.1016/S0032-0633(00)00145-8

Woch, J., Krupp, N., Lagg, A., Wilken, B., Livi, S., and Williams, D. J. (1998). Quasi-periodic modulations of the Jovian magnetotail. *Geophys. Res. Lett.* 25, 1253.

Zarka, P. (2004). Radio and plasma waves at the outer planets. *Adv. Space Res.* 33, 2045–2060. doi: 10.1016/j.asr.2003.07.055

Zieger, B., and Hansen, K. C. (2008). Statistical validation of a solar wind propagation model from 1 to 10 AU. *J. Geophys. Res.* 113, A08107. doi: 10.1029/2008JA013046

Zieger, B., Hansen, K. C., Gombosi, T. I., and De Zeeuw, D. L. (2010). Periodic plasma escape from the mass-loaded Kronian magnetosphere. *J. Geophys. Res.* 115, A08208. doi: 10.1029/2009JA014951